PAPER

Check for updates

Biologically inspired, catechol-coordinated, hierarchical organization of raspberry-like calcium phosphate nanospheres with high specific surface area†

Xiaomin Ma, [ID] [a] Zhe Sun, [a] Wen Su, [ID] [a] Zeng Yi, [ID] [a] Xinxing Cui, [a] Bo Guo*[b] and Xudong Li [ID] *[a]

The elaborate design of calcium phosphates (CaP) with a hierarchical structure for biomedical applications is severely restricted due to their instinctive pertinacious irregular agglomeration. Thus, the development of mesoporous CaP with large internal pores is far from satisfactory. In this study, catechol is selected as a modifier to intervene in the precipitation of CaP. Compared to pure CaP with smooth irregular aggregates with an average size of 110 nm, the catechol-intervened CaP (CaP/Cat) samples are raspberry-like nano-spherical assemblies of *ca.* 25 nm nanoparticles. The obtained spheres possess a mesoporous structure, large interior pores and high specific surface area, which endow them with a high protein adsorption capacity and high DNA delivery efficacy. Catechol is subjected to oxidative polymerization while CaP precipitation occurs. This simultaneous reaction is supposed to play a crucial role in directing the assembling of the CaP/Cat nanospheres. The flexible catechol moiety is shown to be a novel and promising modifier for manufacturing CaP with tunable structures and properties for various applications.

1. Introduction

The rational design and construction of hierarchically organized materials are considered as versatile strategies to achieve unique properties for a variety of functional purposes. In biological systems, highly sophisticated biominerals are well-known examples, which adopt complex hierarchical structures together with a delicate combination of organic and mineral phases for functions ranging from skeletal support and nutrient transport to signal transduction.[1,2] The formation of these biominerals involves exquisitely orchestrated biomineralization processes, which allow the combination of organic and inorganic components at the nanoscale. The indispensable roles of biomolecules in biomineralization have inspired researchers to introduce different modifiers for the preparation of various advanced materials through carefully controlled organic–inorganic interfaces.[3–7] The hierarchical construction of nano/meso-porous architectures especially with a high specific surface area and large pores is of great interest due to the wide applications of these architectures in the fields of catalysis, separation, energy and biomedicine.[8–12]

Calcium phosphates (CaP, primarily apatitic CaP) have inimitable advantages over other inorganic materials because apatitic CaP is bio-safe as the main constituent of the mineral phase of hard tissues in mammals. Nowadays, the preparation of CaP nanostructures is a focus for various biomedical purposes such as bone replacement, protein adsorption, growth factor and anticancer drug delivery and gene transfection.[13–16] To date, many CaP nanostructured architectures have been reported, which are either nanostructures (rods, tubes and spheres)[17–22] or architectures with a hierarchical structure (microspheres and spherulites).[23–27] The generally-applied methods to achieve these nanostructures or hierarchical architectures include hydrothermal reaction,[22,28] sol–gel synthesis,[29] chemical precipitation,[30,31] and the micro-emulsion technique.[32] Among them, soft chemistry and hard templating are used to tackle the pertinacious agglomeration of CaP in solution, whereas soft chemistry associated with the use of organic modifiers, such as macromolecules,[14,33] amino acids,[21] and even proteins,[34] is considered as a mainstream, efficient and bio-mimetic means to control the resulting CaP from solution with tunable crystallinity, morphology and size. Chen *et al.*[19] reported the synthesis of 40 nm monodisperse CaP hybrid nanospheres

[a] *National Engineering Research Center for Biomaterials, Sichuan University, Chengdu 610064, P. R. China. E-mail: xli20004@yahoo.com; Fax: +86-28-85412102; Tel: +86-28-85412102*

[b] *Department of Ophthalmology, West China Hospital, Sichuan University, Chengdu 610041, P. R. China. E-mail: guobohx@163.com*

† Electronic supplementary information (ESI) available. See DOI: 10.1039/c7tb03156d

This journal is © The Royal Society of Chemistry 2018

J. Mater. Chem. B, 2018, **6**, 3811–3819 | 3811

via the segregation crystallization imposed by hyaluronan molecules. In contrast, the self-assembly of CaP nanoparticles into nanoarchitectures is relatively less reported because the self-assembly process further requires the coordinated interaction between the minimization of the nanoparticle surface energy and the rearrangement of organic species absorbed on or incorporated into the inorganic nanoparticles.[6] Tang *et al.*[35] obtained *ca.* 5 nm apatite CaP spheres using poly(acrylic acid) (PAA) as a stabilizing agent in supersaturated CaP solution, where upon the removal of PAA, these nanospheres formed 30 nm colloidal aggregates, which were unstable and de-aggregated and reorganized with moldable amorphous phases. Upon further modulation with glycine (Gly) and glutamic acid (Glu), highly ordered enamel- and bonelike apatites were formed, respectively. Epple *et al.*[36] revealed that in the presence of dissolved amino acids and dipeptides, CaP nanoparticles simultaneously assembled within a few seconds into hollow spheres with a diameter of around 200–300 nm. However, in contrast to the striking achievement of preparing silica, zeolites and related mesoporous materials,[10,37–39] the achievement of hierarchically organized CaP with a high surface area and large pores is far from satisfactory due to the obstinate inherent agglomeration of CaP in solution. The reported CaP with a high surface area also primarily relies upon microemulsion, hydrothermal reaction and hard templating techniques. For example, Uota *et al.*[17] reported the synthesis of CaP nanoparticles with a high surface area *via* the calcination of lath-shaped precursors encapsulated with calcium stearate using surfactant-containing reaction mixtures. Walsh and Mann[23] prepared microskeletal forms of CaP from supersaturated bicontinuous microemulsions. Jiang *et al.*[26] fabricated hollow hydroxyapatite microspheres through a water-soluble biopolymer assisted assembly from CaP nanorods. Recently, He *et al.*[34] used mesoporous silica nanoparticles as a nucleation template and fetuin as an inhibiting agent to prepare mesoporous CaP rod-like nanocrystals with large pores. However, to date, the use of organics for CaP precipitation leading to the self-assembly of nanoparticles into raspberry-like nanostructures has not been reported.

Catechol is the structural unit in a wide variety of naturally occurring hormones, neurotransmitters and polyphenols. Due to the reactivity of the functional catechol group, catecholic chemistry is now emerging as a captivating subject of great importance in the design of adherent materials, inorganic/organic hybrids and functional polymeric materials with unique properties. Since the pioneering discovery of the versatile adhesion of catechols in mussels by Waite and Tanzer in 1981,[40] mussel-inspired biomimetics has revealed their superior ability to form a wide range of interactions with organic and inorganic components.[41] In addition to their use in adhesive interfaces,[42,43] biomimetic molecules possessing the catechol structural unit have also been demonstrated to effectively modulate the precipitation of several inorganic materials.[37,44,45] On the other hand, as a powerful building block for polymeric materials, the catechol moiety can be oxidatively polymerized for the encapsulation of guest molecules and for enhanced delivery of anticancer drugs.[46–48]

In the present study, catechol is used to form a mineralization system at ambient environment and hierarchically organized CaP nanospheres with a tunable architectural structure are prepared using an NH_4OH diffusion method.

2. Experimental

2.1 Materials

All chemicals including catechol, (>99%, Sigma-Aldrich), calcium chloride (Vetec™ reagent grade, 96%, Sigma-Aldrich), sodium phosphate monobasic dihydrate (Vetec™ reagent Grade, ≥99%, Sigma-Aldrich), and concentrated ammonia (25%, w/w%, Kelong, China) were used as received without further purification. Ultra-purified water (18.2 MΩ cm) was used to prepare all aqueous solutions. Fibrinogen (Fib, Sigma-Aldrich, dimensions $9 \times 47.5 \times 6$ nm, pI 5.2, $M_W = 340$ kDa), bovine serum albumin (BSA, lyophilized powder, 99%, Aokesw Biological, dimensions $4 \times 4 \times 14$ nm, pI 4.8, $M_W = 67$ kDa) and lysozyme (Lz from chicken egg white, Ultra-Pure Grade, Solarbio, diameter 3.2 nm, pI 11.4, $M_W = 14$ kDa) were collected as model proteins. The BCA Protein Assay Kit was purchased from Thermal Scientific. Human osteosarcoma cells MG63 were purchased from West China Medical Center of Sichuan University. Dulbecco's Modified Eagle's Medium with high glucose (DMEM-HG) was purchased from GE Healthcare Science (Hyclone, USA) and fetal bovine serum (FBS) was purchased from Life Technologies Corporation (Gibco, USA). Plasmid DNA (pEGFP) was extracted from cultured *E. coli* with a plasmid extraction kit (Invitrogen). Branched polyethyleneimine (PEI, M_W 25 kDa), and antibiotics were obtained from Sigma-Aldrich (USA). 3-(4,5-Dimethylthiazol-2-yl)-2,5-diphenyltetrazolium bromide (MTT) was purchased from Amresco (USA).

2.2 Instruments

The morphology of the nanospheres was investigated with an S-4800 field-emission scanning electron microscope (SEM, Hitachi, Japan) and a Tecnai G² F20 S-TWIN transmission electron microscope (TEM, FEI, USA) at an acceleration voltage of 5 kV and 200 kV, respectively. Nitrogen adsorption and desorption isotherms were measured at 77 K using a Quantachrome NOVA 4200e. The surface area and pore size distribution calculations were based on the Brunauer–Emmett–Teller (BET) and Barrett–Joyner–Halenda (BJH) methods, respectively. Organic elemental analysis (OEA, Thermo Flash EA 1112 Flash 2000, USA) was conducted to detect the existence and percentages of carbon (C), hydrogen (H) and nitrogen (N) in the synthesised samples. Their phase composition was analyzed on a DX-1000 X-ray diffractometer with Cu Kα radiation ($\lambda = 1.5406$ Å) in the 2θ range of 10–70° at a scanning rate of 0.06° s⁻¹. Molecular species were identified *via* Fourier transform infrared spectroscopy (FTIR) using KBr pellets. The spectra were recorded on a Perkin-Elmer Spectrum One B System in the range of 4000–400 cm⁻¹ with a scanning resolution of 2.00 cm⁻¹. A microplate reader (Bio-Teklnstru-ments Inc., USA) was used to quantitate the cell viability and absorbed proteins.

3812 | *J. Mater. Chem. B*, 2018, **6**, 3811–3819

This journal is © The Royal Society of Chemistry 2018

2.3 Preparation of CaP/Cat nanospheres

The calcium phosphate precipitates were synthesized using an NH_4OH diffusion method (ESI,† Fig. S1). Various samples were synthesized with different catechol concentrations and the parameters are shown in Table S1 in the ESI.† In a typical procedure, 1.0 g catechol was dissolved in 60 mL H_2O in a flask placed in a large vessel, and 20 mL 10 mM $CaCl_2$ solution was then added with stirring to the catechol solution followed by the addition of 20 mL 6 mM $NaH_2PO_4 \cdot 2H_2O$ solution, yielding a CaP feedstock solution with the catechol concentration of 1.0 w/v%. Another flask was filled with 100 mL fresh 10% ammonia and subsequently placed at room temperature (RT) in the large vessel, which was sealed with plastic film to initiate the CaP crystallization. The vessel was left to stand in a fume cupboard for 30 minutes prior to collecting the precipitates. Finally, the precipitates were collected by centrifugation, rinsed with deionized water thoroughly (monitoring with conducti-metric measurements) and dried at 60 °C in an oven for further analysis. In the present study, four groups of CaP precipitates were prepared from feedstock solutions containing different catechol concentrations of 0.2, 0.5, 1.0 and 2.0 w/v%, which were denoted as CaP/Cat-0.2, CaP/Cat-0.5, CaP/Cat-1.0 and CaP/Cat-2.0, respectively. CaP was also synthesized without catechol as a control, which was denoted as control CaP.

2.4 Protein adsorption of control CaP and CaP/Cat-1.0 mesoporous spheres

The CaP/Cat-1.0 nanospheres were used for the adsorption of proteins. Accordingly, the protein adsorption rate was determined by monitoring the amount of protein absorbed by CaP/Cat-1.0 mesoporous spheres for 48 h in PBS. PBS (10 mM, pH = 7.4) was prepared freshly. A total of 60 mg CaP/Cat-1.0 mesoporous spheres were dispersed in 6 mL PBS and the colloidal solution was divided into three 2 mL aliquots. Individual stock solutions (4 mg mL^{-1}) of Fib, BSA, and Lz were prepared using the same PBS solution, and 2 mL of each was added to an equal volume of CaP/Cat-1.0 mesoporous spheres, followed by incubation for 48 h at room temperature. 200 μL aliquots were periodically removed and centrifuged, and the supernatant was analyzed using the BCA Protein Assay Kit (Thermal Scientific) and quantified on a microplate reader. The protein adsorption of control CaP was tested similarly.

2.5 Gene transfection

Complexes of DNA (pEGFP) and the CaP/Cat-1.0 mesoporous spheres were prepared by adding 0.5 μL $CaCl_2$ (0.25 M) solution and 2 μL DNA (100 ng μL^{-1}) solution to 10 μL colloidal solution of CaP/Cat-1.0 (0.1 mg mL^{-1}), which were incubated at room temperature for 20 min before use. Commercial transfection reagent, PEI, was used as a positive control for comparison. DNA/PEI binary complexes were prepared by mixing DNA and PEI solution gently at an N/P ratio of 10, which were incubated under the same conditions as DNA/CaP/Cat-1.0. All biological experiments were conducted in quintuplicate. MG63 cells were maintained in Dulbecco's Modified Eagle's Medium (DMEM) supplemented with 10% fetal bovine serum (FBS), penicillin (100 units mL^{-1}) and streptomycin (100 mg mL^{-1}) at 37 °C and 5% CO_2. For the transfection study, MG63 cells were seeded at a density of 0.8×10^4 cells per well in 96-well plates and grew to 70–80% cell confluence. Before transfection, the medium was removed, and the cells were washed and replaced with 100 μL DMEM without FBS. The DNA/CaP/Cat-1.0 complexes and DNA/PEI complex were respectively added to each well. The amount of DNA was kept constant at 200 ng DNA per well and the cells were incubated with the above complexes at 37 °C for 4 h. The medium was then replaced with DMEM supplemented with 10% FBS and the cells were incubated for an additional 48 h. pEGFP gene transfection was visualized with a fluorescence microscope. For the cytotoxicity assay, the cells were washed with PBS after incubation for 48 h, and then 50 μL of 2 mg mL^{-1} MTT solution in PBS was added to each well. After incubating the cells for another 4 h at 37 °C, the MTT-containing medium was removed and 100 μL of DMSO was added to dissolve the formazan crystals formed by the living cells. The cells incubated with DMEM only was set as the control. Absorbance was measured at 490 nm using a microplate reader (Bio-Teklnstru-ments Inc., USA).

3. Results and discussion

3.1 Architecture and applications

The representative TEM image of the CaP precipitates obtained in CaP/Cat-1.0 (Fig. 1A) shows a unique framework structure, as revealed by the differentiated electron density across the circular objects observed. Despite the projection nature of TEM observations, the examined samples present a hierarchically reticulated architecture with excellent interconnectivity. This prominent feature of the TEM image is beyond that reported for many mesoporous materials.[37] Nitrogen sorption measurement was applied to characterize the reticulated framework of these nanospheres. According to the nitrogen adsorption–desorption isotherm (Fig. 1B), these nanospheres exhibit a type IV isotherm with a distinct hysteresis loop, which confirms the existence of an inherent mesoporous structure. The Brunauer–Emmett–Teller (BET) surface area and pore volume of the nanospheres are 217.378 m^2 g^{-1} and 0.644 cm^3 g^{-1}, respectively, which values are both much higher than that of the as-prepared products reported for CaP nano- and micro-particles.[32] These results may be derived from the inner structure of the CaP/Cat-1.0 nanospheres. CaP/Cat-1.0 possesses raspberry-like spheres composed of 25 nm CaP nanoparticles with high interparticle porosity (shown in Fig. 2), which endow the nanospheres with high surface area. The comparison of the control particles with a diameter of 126.3 nm to that of 25 nm in CaP/Cat-1.0 in the TEM and SEM images indicates the inhibitory effect of catechol on the growth of large crystallites during the precipitation of CaP, which results in a high surface area.[49] The pore size distribution was calculated based on the Barrett–Joyner–Halenda (BJH) method using the desorption portion of the nitrogen adsorption–desorption isotherm. The BJH pore diameter distribution curve

This journal is © The Royal Society of Chemistry 2018
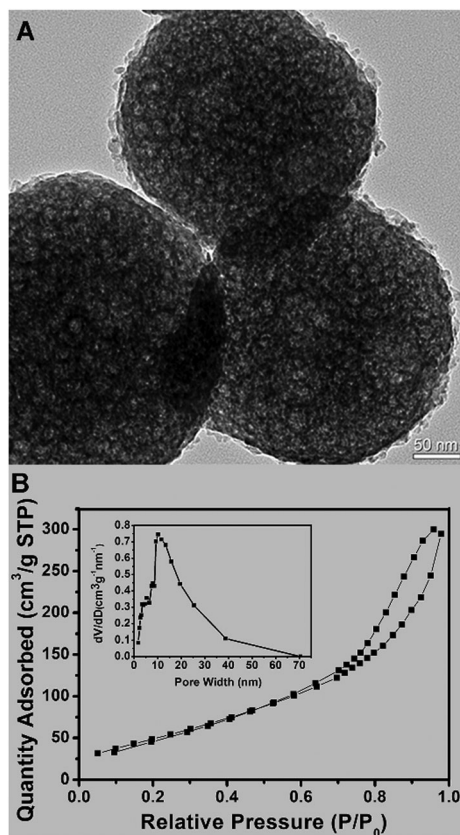
J. Mater. Chem. B, 2018, 6, 3811–3819 | 3813

Fig. 1 Morphology and interior structure of CaP/Cat-1.0. (A) TEM and (B) nitrogen adsorption−desorption isotherm and (inset) pore distribution curve.
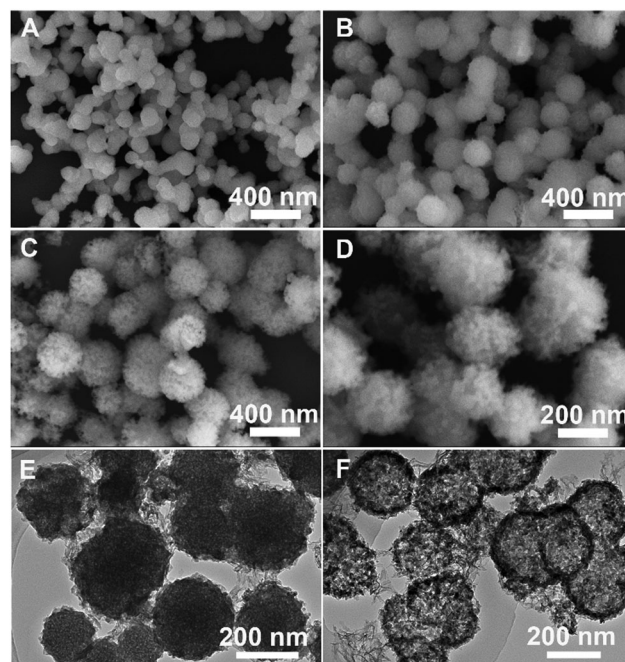

Fig. 2 SEM images of CaP/Cat nanospheres: (A) CaP/Cat-0.2, (B) CaP/Cat-0.5, (C) CaP/Cat-1.0 and (D) a magnified view of (C). TEM images of (E) CaP/Cat-0.5 and (F) CaP/Cat-2.0.

(the inset in Fig. 1B) clearly shows a multi-modal (*e.g.*, *ca.* 5.0, 8.0 and 10.0 nm) distribution of pores, which is mainly distributed around 10.0 nm, and the average pore size is 7.273 nm. The multi-modal pore distribution is due to the fantastic combination of internal and external pores with varying dimensions among particles, which is in good agreement with the TEM observations. The hysteresis loop recorded at a higher relative pressure supports the existence of interparticle porosity. The formation of an open porous interconnected three-dimensional network spatially confined to <300 nm spheres with a high surface area permits biomedical applications for the encapsulation of guests, especially larger sized biomacromolecules.

The control CaP precipitates are irregular aggregates composed of *ca.* 126.3 nm sized nanocrystals (Fig. S2, ESI†). In contrast, a significant change in the morphology of the precipitates is observed in the CaP/Cat samples synthesized with the introduction of catechol. In the case of the CaP/Cat-0.2 sample, which was synthesized at the lowest catechol concentration of 0.2 wt%, the precipitates are spheroidal particles, but some spheroidal particles fuse to form a bridging structure (Fig. 2A). The size of these spheroidal particles ranges from 52.2 nm to 183.8 nm, with the average diameter of 134.2 nm. A well-defined spherical morphology is observed in the CaP/Cat-0.5 precipitates (Fig. 2B). In accordance with the improved sphericity and the decreased fusion of particles, the average

diameter of these CaP/Cat-0.5 spheres increases up to 231.1 nm. When the concentration of catechol was increased to 1.0 wt% during CaP precipitation, surface roughening becomes the salient feature of the CaP/Cat-1.0 spheres with an average size of 275 nm (Fig. 2C). In fact, the surface roughening extent continuously increases in the precipitates obtained with a higher concentration of catechol compared with the smooth surface of the irregular aggregates in the control CaP precipitates. Also, as the catechol concentration increases, the uniformity of the particle size increases. The CaP/Cat-1.0 spheres are hierarchical raspberry-like nanospheres due to the presence of many villi and small spheroids (Fig. 2D), which result in the rough surface. It is worth noting that the small spheroids are only *ca.* 25 nm, which is much smaller than the basic nanocrystals (*ca.* 126.3 nm) of the control CaP. According to the TEM image of the CaP/Cat-1.0 sample (Fig. 1A), the observed nanoskeletal structure is actually a hierarchical spherical architecture organized by many fluffy nanospheroids. Interestingly, the biomineralization in the pineal gland of humans and animals (pineal calcification) also yields similar structures but with dimensions in the order of hundreds of micrometers,[50] which consist of a mineral component, hydroxyapatite or calcite, and protein and glycoprotein organic components. The similarity between the pineal microcrystals and present CaP/Cat nanospheres suggests that the role of catechol in controlling CaP is analogous to the functions of acidic glycoprotein to some degree. The self-assembly of these small spheroids into spherical nanostructures is also observed in the CaP/Cat-2.0 precipitates (Fig. S3, ESI†) as looser assemblies 196.6–312.5 nm in diameter. The presence of incomplete spherical objects (the inset in Fig. S3, ESI†) additionally reveals the hierarchically organized

Table 1 BET surface area, pore volume and pore size of the CaP/Cat nanospheres from the nitrogen sorption measurements

Samples	BKT surface area, $m^3\ g^{-1}$	Pore volume, $cm^3\ g^{-1}$	Pore size, nm
CaP/Cat-0.2	41.497	0.087	2.459
CaP/Cat-0.5	99.856	0.321	2.431
CaP/Cat-1.0	*217.378*	*0.644*	*7.273*
CaP/Cat-2.0	37.321	0.103	2.782

structure. The TEM images of the CaP/Cat-0.5 and CaP/Cat-2.0 samples (Fig. 2E and F) show a reticulated internal structure and an approximately hollow structure, respectively.

To further characterize the porosity of the CaP–Cat samples, we conducted nitrogen adsorption–desorption measurements. The BET surface area, pore volume and pore size of the CaP/Cat samples are presented in Table 1. The results indicate that the CaP/Cat nanospheres possess nonuniform pores, and a high surface area and pore volume. Also, it is obvious that these parameters are catechol concentration-dependent, where a high catechol concentration results in large pores and high surface area. However, this trend is altered when the concentration of catechol increases to 2.0%. The BET surface area, pore volume and pore size all decreased dramatically to a level similar to that of CaP/Cat-0.2, which could be attributed to the hollow structure of CaP/Cat-2.0. In detail, the hollow spheres are assembled of comparably less nanoparticles, leading to less interspaces between the assembled units.

3.2 Adsorption of proteins

The porous structure of the nanospheres makes them promising candidates as macromolecule carriers. The obtained CaP/Cat-1.0 NPs exhibit large pores and a high specific surface area, and thus were selected to test the capability of loading guest proteins in PBS. Accordingly, the mean particle size and zeta potential of each sample were characterized and the results are presented in Table S1 (ESI†). The DLS result of control CaP is invalid due to its aggregation, while the CaP/Cat samples show good results, where their mean sizes are consistent with the SEM observation. Also, the zeta potential of control CaP, CaP/Cat-0.2, CaP/Cat-0.5, CaP/Cat-1.0 and CaP/Cat-2.0 is +0.4, −11.8 mV, −14.0 mV, −14.6 mV and −10.1 mV, respectively. The size of the CaP/Cat particles is suitable for the transport of biomacromolecules and their negatively charged surface is beneficial for the adsorption of positively charged molecules. Three different types of proteins, albumin (BSA), lysozyme (Lz) and fibrinogen (Fib), were selected as model proteins. The adsorption kinetic curves (Fig. 3A) indicate the fast adsorption of the proteins onto/into the CaP nanospheres, and stable equilibrium adsorption is maintained during the incubation up to 48 hours. The equilibrium adsorption capacity of the proteins on the CaP/Cat-1.0 nanospheres (Fig. 3B) is 395.9 mg g^{-1} for Fib, 334.2 mg g^{-1} for BSA and 125.0 mg g^{-1} for Lz, while the adsorption of the proteins on the control CaP finished almost instantly in 5 min with values of 375.0 mg g^{-1} for Fib, 254.9 mg g^{-1} for BSA and 14.6 mg g^{-1} for Lz. The values for CaP/Cat-1.0 are quite high compared to the control CaP and the reported results achieved with
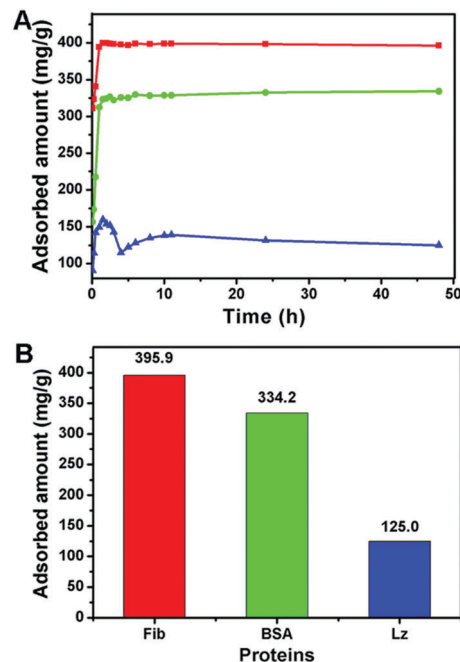
Fig. 3 (A) Proteins adsorption kinetics for CaP/Cat. Fib (red), BSA (green) and Lz (blue) and (B) respective equilibrium protein adsorption capacity.

CaP nanoparticles[34,51] and silica nanoparticles.[37] Fib possesses the largest molecular weight, thus equal adsorption with other proteins will lead to more adsorbed weight for Fib. Therefore, both control CaP and CaP/Cat-1.0 show the highest capacity for Fib. The negatively charged surface of the CaP/Cat-1.0 nanospheres significantly differs from that of the control CaP nanoparticles, leading to a remarkable increase in the adsorption of Lz. In addition, the organic species of catechol has high affinity to proteins, thus CaP/Cat-1.0 shows a higher capacity for each protein.[37] Apart from the specific surface of CaP, its inner structure is also related to its kinetics and capacity for proteins. The dense and smooth properties of control CaP led to the fast adsorption of each protein, while a fluctuation occurred in the adsorption of Lz in the CaP/Cat-1.0 group. This may originate from the desorption and subsequent diffusion of Lz molecules into the CaP/Cat-1.0 pores. Thus, the high capacity for protein adsorption of the CaP/Cat-1.0 nanospheres can be attributed to their rough and negatively charged surface and porous interstructure, which verifies their potential applications as carriers for functional proteins in the biomedical field.

3.3 Gene transfection

Furthermore, we evaluated the potential of the CaP/Cat-1.0 nanospheres as a gene vector for DNA loading and *in vitro* transfection with reference to the branched polyethyleneimine (PEI, M_W 25 kDa). The successful transfection was confirmed by fluorescence microscopy, where the fluorophore protein EGFP was excited inside cells (Fig. 4A). From the fluorescence microscopy images, it can be seen that the CaP/Cat-1.0 group shows a similar transfection efficiency with the PEI group (seen in Fig. S4, ESI†). However, the MTT assays confirm that the DNA complexes with the CaP/Cat-1.0 nanospheres are biological safer than that
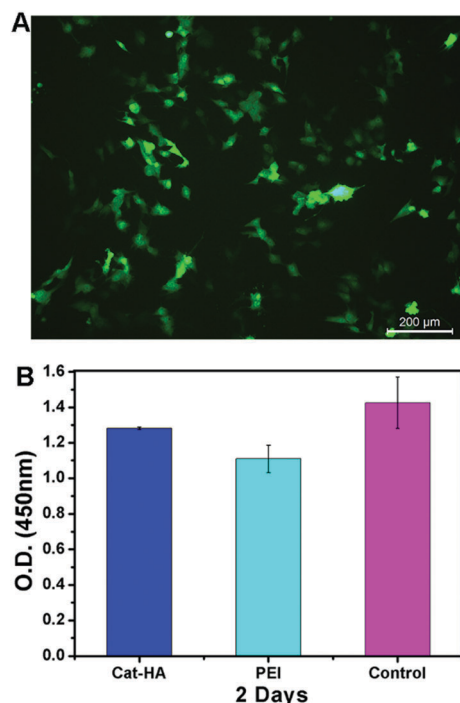
Fig. 4 (A) EGFP fluorescence microscopy images of MG63 cells transfected with CaP/Cat-1.0 nanospheres (transfected cells appear green) and (B) MTT assay cell viability results of MG63 cells incubated with DNA complexes of CaP/Cat-1.0 and PEI_{25k}.
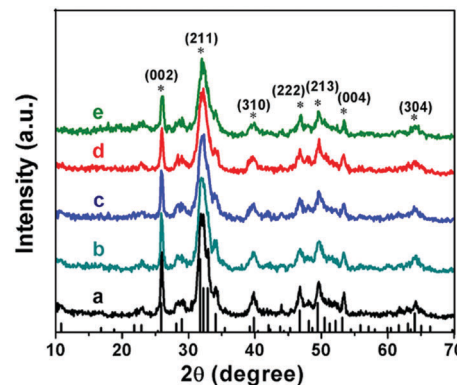

Fig. 5 XRD patterns of the CaP precipitates obtained from feedstock solutions in the presence of varying concentrations of catechol: (a) control CaP, (b) CaP/Cat-0.2, (c) CaP/Cat-0.5, (d) CaP/Cat-1.0 and (e) CaP/Cat-2.0.
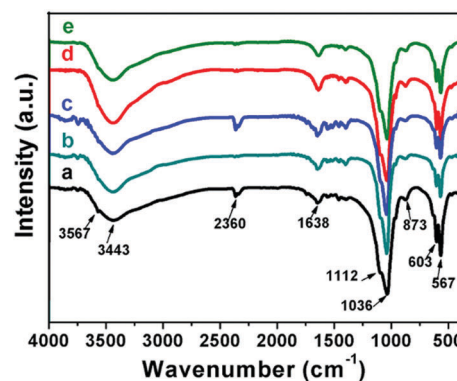

Fig. 6 FT-IR spectra of the CaP/Cat precipitates obtained from feedstock solutions in the presence of varying concentrations of catechol: (a) control CaP, (b) CaP/Cat-0.2, (c) CaP/Cat-0.5, (d) CaP/Cat-1.0 and (e) CaP/Cat-2.0.

with PEI (Fig. 4B). The results indicate that the synthesized CaP/Cat NPs are potentially effective and biocompatible gene transfer-agents.

3.4 Structural confirmation

All the samples obtained from feedstock solutions in the absence (Control CaP) and presence of different concentrations of catechol (CaP/Cat-0.2, CaP/Cat-0.5, CaP/Cat-1.0, and CaP/Cat-2.0) have similar XRD traces (Fig. 5). Their reflections well coincide with the standard data of HA (JCPDS card No. 09-0432), confirming that the precipitates have the apatite structure. The reflections located at $2\theta = 26.0°$, $31.9°$, $39.8°$, $46.7°$, $49.7°$, $53.2°$ and $64.2°$ are assigned to the (002), (211), (310), (222), (213), (004) and (304) planes of hydroxyapatite, respectively. Compared with control CaP, the CaP/Cat precipitates obtained with a higher concentration of catechol possess relatively lower crystallinity, suggesting that catechol follows a concentration-dependent trend to inhibit CaP crystallization. This conclusion is supported by the gradual decrease in the sharpness of all the reflections and in the half-height-width value of the (002) plane from (a) (Control CaP) to (e) (CaP/Cat-2.0) in Fig. 5.

The FT-IR spectra show several characteristic absorptions for CaP (Fig. 6). The absorptions at 603 and 567 cm^{-1} belong to the triply degenerated bending mode of the O−P−O bonds of the phosphate group, while its asymmetric stretching mode appears at 1036 cm^{-1}. In general, the stretching vibrations of the hydroxyl group of CaP give absorptions at 631 and

3560 cm^{-1}, and the detection and the sharpness of these absorptions are related to the ordering extent of the synthetic CaP crystals. The absence of the absorption at 631 cm^{-1} confirms the poor crystallization feature of the precipitates obtained at room temperature in the present study. In particular, a very weak absorption at 3567 cm^{-1} is observed only in the control CaP sample, which further verifies the XRD result that the CaP control has the highest crystallinity among the precipitates. It is worth noting that the characteristic sharp absorptions in the fingerprint region of catechol are absent in the CaP/Cat samples, indicating the restriction of the stretching and bending vibrations of catechol. This phenomenon could be attributed to the oxidative coupling oligomerization of catechol.[44] It is reported that the alkaline conditions, air and presence of Ca^{2+} in this reaction system contribute to accelerating catechol oxidation.[52,53] This restrictive effect also explains why catechol could not be definitely identified in the FT-IR spectra of the CaP/Cat precipitates since the phenol groups at $ca.$ 3430 cm^{-1} and aromatic rings at 1630 cm^{-1} also overlapped with the hydroxyl groups of apatite CaP and adsorbed water. OEA (Organic Elemental Analysis) characterization of control CaP and CaP/Cat-1.0 was also performed to prove the presence

3816 | J. Mater. Chem. B, 2018, 6, 3811–3819

This journal is © The Royal Society of Chemistry 2018

of organics in the final rinsed sample. The results show that the percentages of C (carbon) and H (hydrogen) in CaP/Cat-1.0 are 1.48% and 0.59%, respectively, which are significantly higher than that of 0.48% and 0.47% in control CaP, respectively. Considering the dissolution of carbon dioxide in water, we attribute the 0.48% of C in control CaP to CO_2. The percentage of C in CaP/Cat-1.0 is 1.0% higher than that in control CaP, which confirms the inclusion of catechol instead of only low residual coverage in the nanospheres. During the reaction, the reaction solutions turned brown, indicating the oxidation of catechol.[54,55] The collected CaP/Cat samples present a greyish color, as seen in Fig. S5 (ESI†), despite repeated washing with water, which confirms the hybrid of oxidized catechol and CaP. The zeta potential of the CaP/Cat-1.0 nanospheres is -14.6 mV (Table S1, ESI†), whereas this value for pure CaP is 0.4 mV. This further confirms the effect of catechol molecules on the synthetic CaP/Cat nanospheres.

3.5 Possible mechanism

The intervention of inorganic or organic modifiers into CaP synthetic solutions provides opportunities to control the emerging behavior of the CaP solution and the densification/maturation of the emerging clusters *via* ionic exchange of the labile environments on a hydrated layer at the surface of the CaP clusters for the rational design and preparation of ideal CaP nanostructures. Catechol is a variable species in ambient environment. The vicinal di-hydroxy structures of catechol are known to contribute to the chelation of metals such as Ca^{2+} and also to be susceptible to air oxidation.[47,52,56] The previous synthesis of CaP nanoparticles using polyphenol was achieved under the protection of nitrogen gas.[57] In contrast, simultaneous catechol autoxidation during CaP precipitation is believed to be crucial for the formation of raspberry spheres assembled by nanoparticles in this study. Herein, based on the present sample characterization, we tentatively give the following molecular mechanism for the self-assembly of nanoparticles into raspberry-like spheres coordinated with catechol, which is further illustrated schematically in Fig. 7. Under an aerobic environment, the autoxidation of catechol occurs with the simultaneous synthesis of CaP in the present study. As Ca^{2+}–catechol complexation (Ca^{2+}–Cat^{2-}) occurs, even with weak acids, additional deprotonation of catechol molecules is provoked, which accelerates the autoxidation of catechol (Fig. 7A). The abundant catecholate moieties initiate the formation of numerous CaP particles, which emerge from and are stable in solution, thus avoiding the rapid growth of CaP agglomerates in the absence of catechol.

The aggregation growth further proceeds with the prolonged reaction. At this stage, the minimum surface energy principle governs the formation of raspberry-like spherical assemblies of *ca.* 25 nm nanoparticles. The self-assembly of these nanoparticles into nanospheres is mainly driven by the molecular entanglements and intermolecular forces of the oligomerized catechol species on the surface of the fluffy nanoparticles, probably such as hydrophobic interactions and H-bonds.[6,47] The modulating effect of the catecholic molecules in the
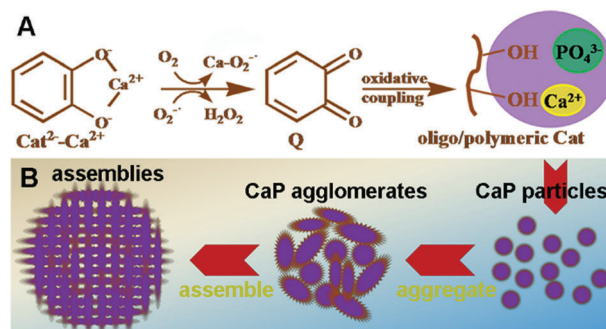

Fig. 7 Possible molecular mechanism for the self-assembly of nanoparticles into raspberry-like spheres coordinated with catechol.

synthesis of CaP follows a concentration-dependent manner, as revealed by the SEM, TEM, XRD and FT-IR analyses (Fig. 2, 5 and 6, respectively). To achieve the integral architecture assembled by nanoparticles, the optimal concentration of catechol is required to secure the stability of the internal structure by initiating adequate molecular interactions. According to the TEM observations, the hierarchically reticulated architecture was achieved in the CaP/Cat-1.0 nanospheres (Fig. 1A). In contrast, the final CaP/Cat-2.0 precipitates are actually hollow nanospheres (Fig. 2). It is noteworthy that the present catechol-intervened precipitation process of CaP is also accompanied by the *in situ* polymerization of the modifiers, *i.e.*, the simultaneous autoxidation of catechol molecules. This dynamic process is quite different with the conventional biomimetic approaches using organic modifiers such as biomacromolecules. Their modulating effects are realized generally *via* the molecular interactions of the cations and/or anions of the inorganic sources with the active groups and the relevant coil/loop conformations of flexible molecular chains attached to the stable skeletal structure of biomacromolecules.[19,58] Therefore, this study not only successfully prepares nanosized spheres with hierarchically reticulated architectures assembled by nanoparticles for various biomedical purposes, but also offers an innovative strategy for the biomimetic study of biomineralization.

4. Conclusions

We reported the successful preparation of dispersed spherical CaP nanoarchitectures hierarchically assembled by nanoparticles based on the intervention of a varying concentration of catechol in CaP precipitation under ambient conditions. When the concentration of catechol was 1.0 wt%, a hierarchically reticulated architecture with excellent interconnectivity was obtained in the CaP/Cat-1.0 precipitates. These raspberry-like CaP/Cat-1.0 nanospheres, less than 300 nm in diameter, are raspberry-like architectures assembled by *ca.* 25 nm sized nanoparticles, having a high BET surface area (217.38 m^2 g^{-1}) with pores up to 10 nm in size. We demonstrated that these nanospheres have high protein adsorption capacity for Fib (395.9 mg g^{-1}), BSA (334.2 mg g^{-1}) and Lz (125.0 mg g^{-1}) and

This journal is © The Royal Society of Chemistry 2018

J. Mater. Chem. B, 2018, 6, 3811–3819 | 3817

are bio-safe for the successful application of gene transfection. The presence of catechol is shown to reduce the crystallinity of CaP and to initiate the assembling of the nanoparticles. Meanwhile, the morphological development of the raspberry-like nanospheres follows a catechol concentration-dependent fashion, *i.e.*, the nanospheres become more dispersed and more loosely assembled with an increase in size with a higher concentration of catechol. The simultaneous autoxidation of catechol molecules during the precipitation of CaP is believed to be crucial for achieving the present self-assembly of nanoparticles into raspberry-like spheres. The requirement of an optimal catechol concentration is further suggested for achieving raspberry-like nanospheres assembled by *ca.* 25 nm nanoparticles, which are promising for various biomedical purposes. The present approach is an innovative and dynamic strategy that combines the *in situ* polymerization of catechol with CaP precipitation.

Conflicts of interest

There are no conflicts of interest to declare.

Acknowledgements

References

1 S. Mann, *Biomineralization: principles and concepts in bioinorganic materials chemistry*, Oxford University Press on Demand, 2001.
2 J. C. Elliott, *FEBS Lett.*, 1990, 149.
3 E. Dujardin and S. Mann, *Adv. Mater.*, 2002, **14**, 775.
4 C. Sanchez, H. Arribart and M. M. G. Guille, *Nat. Mater.*, 2005, **4**, 277–288.
5 F. C. Meldrum and H. Colfen, *Chem. Rev.*, 2008, **108**, 4332–4432.
6 S. Mann, *Nat. Mater.*, 2009, **8**, 781–792.
7 F. Nudelman and N. A. J. M. Sommerdijk, *Angew. Chem., Int. Ed.*, 2012, **51**, 6582–6596.
8 C. Sanchez, C. Boissiere, S. Cassaignon, C. Chanéac, O. Duruphty, M. Faustini, D. Grosso, C. Laberty-Robert, L. Nicole and D. Portehault, *Chem. Mater.*, 2013, **26**, 221–238.
9 Y. Deng, J. Wei, Z. Sun and D. Zhao, *Chem. Soc. Rev.*, 2013, **42**, 4054–4070.
10 Y. Chen, H. Chen and J. Shi, *Adv. Mater.*, 2013, **25**, 3144–3176.
11 V. Di Mauro, M. Iafisco, N. Salvarani, M. Vacchiano, P. Carullo, G. B. Ramirez-Rodriguez, T. Patricio, A. Tampieri, M. Miragoli and D. Catalucci, *Nanomedicine*, 2016, **11**, 891–906.
12 G. Wang, R. Y. Cao, R. Chen, L. Mo, J. F. Han, X. Wang, X. Xu, T. Jiang, Y. Q. Deng, K. Lyu, S. Y. Zhu, E. D. Qin, R. Tang and C. F. Qin, *Proc. Natl. Acad. Sci. U. S. A.*, 2013, **110**, 7619–7624.
13 S. Pina, J. M. Oliveira and R. L. Reis, *Adv. Mater.*, 2015, **27**, 1143–1169.
14 K. Bleek and A. Taubert, *Acta Biomater.*, 2013, **9**, 6283–6321.
15 B. Mostaghaci, B. Loretz, R. Haberkorn, G. Kickelbick and C. M. Lehr, *Chem. Mater.*, 2013, **25**, 3667–3674.
16 W. Wang, Y. Zhao, S. Y. Yang, Q. S. Wu, Y. M. Ju and S. H. Yu, *Inorg. Chem. Front.*, 2017, **4**, 1135–1140.
17 M. Uota, H. Arakawa, N. Kitamura, T. Yoshimura, J. Tanaka and T. Kijima, *Langmuir*, 2005, **21**, 4724–4728.
18 J. Hui, G. Xiang, X. Xu, J. Zhuang and X. Wang, *Inorg. Chem.*, 2009, **48**, 5614–5616.
19 Z. Chen, H. Zhou, X. Wang, L. Sang, C. Wang, J. Ma and X. Li, *Chem. Commun.*, 2010, **46**, 1278–1280.
20 H. J. Lee, S. E. Kim, I. K. Kwon, C. Park, C. Kim, J. Yang and S. C. Lee, *Chem. Commun.*, 2010, **46**, 377–379.
21 T. Matsumoto, M. H. Uddin, S. H. An, K. Arakawa, E. Taguchi, A. Nakahira and M. Okazaki, *Mater. Chem. Phys.*, 2011, **128**, 495–499.
22 Y. M. Wang, X. X. Ren, X. M. Ma, W. Su, Y. P. Zhang, X. S. Sun and X. D. Li, *Cryst. Growth Des.*, 2015, **15**, 1949–1956.
23 D. Walsh and S. Mann, *Chem. Mater.*, 1996, **8**, 1944–1953.
24 Y. Wang, M. S. Hassan, P. Gunawan, R. Lau, X. Wang and R. Xu, *J. Colloid Interface Sci.*, 2009, **339**, 69–77.
25 K. L. Lin, X. G. Liu, J. Chang and Y. J. Zhu, *Nanoscale*, 2011, **3**, 3052–3055.
26 S. D. Jiang, Q. Z. Yao, G. T. Zhou and S. Q. Fu, *J. Phys. Chem. C*, 2012, **116**, 4484–4492.
27 M. G. Ma, *Int. J. Nanomed.*, 2012, **7**, 1781–1791.
28 T. Nomoto, S. Fukushima, M. Kumagai, K. Miyazaki, A. Inoue, P. Mi, Y. Maeda, K. Toh, Y. Matsumoto and Y. Morimoto, *Biomater. Sci.*, 2016, **4**, 826–838.
29 G. Liu, D. Zhao, A. P. Tomsia, A. M. Minor, X. Song and E. Saiz, *J. Am. Chem. Soc.*, 2009, **131**, 9937–9939.
30 L. He, D. Deng, X. Zhou, L. Cheng, J. M. Cate, J. Li, X. Li and W. Crielaard, *J. Biomed. Mater. Res., Part B*, 2015, **103**, 1525–1531.
31 X. Ma, W. Peng, W. Su, Z. Yi, G. Chen, X. Chen, B. Guo and X. Li, *Inorg. Chem.*, 2018, **57**, 4516–4523.
32 H. C. Shum, A. Bandyopadhyay, S. Bose and D. A. Weitz, *Chem. Mater.*, 2009, **21**, 5548–5555.
33 J. J. Donners, R. J. Nolte and N. A. Sommerdijk, *Adv. Mater.*, 2003, **15**, 313–316.
34 Q. J. He, L. M. Pan, Y. W. Wang and F. C. Meldrum, *Cryst. Growth Des.*, 2015, **15**, 723–731.
35 J. Tao, H. Pan, Y. Zeng, X. Xu and R. Tang, *J. Phys. Chem. B*, 2007, **111**, 13410–13418.
36 D. Hagmeyer, K. Ganesan, J. Ruesing, D. Schunk, C. Mayer, A. Dey, N. A. J. M. Sommerdijk and M. Epple, *J. Mater. Chem.*, 2011, **21**, 9219–9223.
37 Z. Gao and I. Zharov, *Chem. Mater.*, 2014, **26**, 2030–2037.
38 L. H. Chen, X. Y. Li, J. C. Rooke, Y. H. Zhang, X. Y. Yang, Y. Tang, F. S. Xiao and B. L. Su, *J. Mater. Chem.*, 2012, **22**, 17381–17403.

3818 | *J. Mater. Chem. B*, 2018, **6**, 3811–3819

This journal is © The Royal Society of Chemistry 2018

39 A. G. Machoke, A. M. Beltrán, A. Inayat, B. Winter, T. Weissenberger, N. Kruse, R. Güttel, E. Spiecker and W. Schwieger, *Adv. Mater.*, 2015, **27**, 1066–1070.

40 J. H. Waite and M. L. Tanzer, *Science*, 1981, **212**, 1038–1040.

41 H. Lee, S. M. Dellatore, W. M. Miller and P. B. Messersmith, *Science*, 2007, **318**, 426–430.

42 J. Ryu, S. H. Ku, H. Lee and C. B. Park, *Adv. Funct. Mater.*, 2010, **20**, 2132–2139.

43 Q. Ye, F. Zhou and W. Liu, *Chem. Soc. Rev.*, 2011, **40**, 4244–4258.

44 S. S. Wang and A. W. Xu, *Cryst. Growth Des.*, 2013, **13**, 1937–1942.

45 Z. H. Chen, C. H. Wang, H. H. Zhou, L. Sang and X. D. Li, *CrystEngComm*, 2010, **12**, 845–852.

46 J. Su, F. Chen, V. L. Cryns and P. B. Messersmith, *J. Am. Chem. Soc.*, 2011, **133**, 11850–11853.

47 Z. Chen, C. Wang, J. Chen and X. Li, *J. Am. Chem. Soc.*, 2013, **135**, 4179–4182.

48 J. E. Chung, S. Tan, S. J. Gao, N. Yongvongsoontorn, S. H. Kim, J. H. Lee, H. S. Choi, H. Yano, L. Zhuo, M. Kurisawa and J. Y. Ying, *Nat. Nanotechnol.*, 2014, **9**, 907–912.

49 S. Ng, J. Guo, J. Ma and S. C. Loo, *Acta Biomater.*, 2010, **6**, 3772–3781.

50 S. Baconnier, S. B. Lang, M. Polomska, B. Hilczer, G. Berkovic and G. Meshulam, *Bioelectromagnetics*, 2002, **23**, 488–495.

51 W. H. Lee, C. Y. Loo, K. L. Van, A. V. Zavgorodniy and R. Rohanizadeh, *J. R. Soc., Interface*, 2012, **9**, 918–927.

52 A. V. Lebedev, M. V. Ivanova, A. A. Timoshin and E. K. Ruuge, *ChemPhysChem*, 2007, **8**, 1863–1869.

53 M. L. Colarieti, G. Toscano, M. R. Ardi and G. Greco, Jr., *J. Hazard. Mater.*, 2006, **134**, 161–168.

54 M. B. Mcbride, F. J. Sikora and L. G. Wesselink, *Soil Sci. Soc. Am. J.*, 1988, **52**, 985–993.

55 F. Russo, M. A. Rao and L. Gianfreda, *Appl. Microbiol. Biotechnol.*, 2005, **68**, 131–139.

56 E. Faure, C. Falentin-Daudre, C. Jerome, J. Lyskawa, D. Fournier, P. Woisel and C. Detrembleur, *Prog. Polym. Sci.*, 2013, **38**, 236–270.

57 R. C. Zhou, S. X. Si and Q. Y. Zhang, *Appl. Surf. Sci.*, 2012, **258**, 3578–3583.

58 T. Tsuji, K. Onuma, A. Yamamoto, M. Iijima and K. Shiba, *Proc. Natl. Acad. Sci. U. S. A.*, 2008, **105**, 16866–16870.